

**FIRST-PRINCIPLES DEFECT CHEMISTRY  
FOR MODELING IRRADIATED GaAs AND III-V SEMICONDUCTOR DEVICES**

Peter A. Schultz

Advanced Device Technologies Department 1425

Sandia National Laboratories, Albuquerque, NM 87185, U.S.A.

**ABSTRACT**

In the absence of direct testing of electronic components under irradiation, a system of experiments and simulations are needed to simulate and predict radiation effects in electronic devices. The physical phenomena responsible for this performance degradation begin with atomic displacements and subsequent chemical evolution of the initial population of defects. The foundation of a multiscale modeling framework for modeling radiation effects in electronics is a quantitative description of these atomic processes. I describe the development of radiation-induced defect chemistries for irradiated GaAs using first-principles quantum chemical methods, with the goal of informing defect physics models needed for continuum-scale device simulations.

**INTRODUCTION**

Transient damage in irradiated semiconductor devices, particularly in the very short times after irradiation, can be severe enough to compromise the operation of crucial electronic components. One of Sandia's scientific interests is to assess the performance of electronics subjected to fast bursts of neutrons. In the absence of direct testing, more limited experiments are augmented with numerical simulations to assess device performance in high radiation environments. To produce quantitatively reliable predictions of system response in irradiated devices, this effort adopts a hierarchical approach, beginning with predictions of atomic defects generated by displacement damage in the initial radiation cascade, and propagating a

quantitative, mechanistic description of the evolving atomic defect chemistry into simulations of electronic devices, in turn feeding device response into reliable predictions of the performance of entire irradiated circuits.

The foundation of the multiscale chain in this science-based approach to modeling radiation damage in electronic devices is accurate description of defect properties: defect formation energies, stable charge states and atomic configurations, defect migration and reaction energies, and electron energy levels. These parameters populate defect physics models necessary to describe the radiation-instigated, evolving defect chemistry and its interaction with charge carriers in device simulations. For silicon-based devices, a vast body of experimental lore provides much of the data concerning defects necessary to populate the defect physics package needed by the device codes [1]. For compound semiconductors, such as GaAs, used in heterojunction bi-polar transistors (HBTs), the post-radiation defect reaction chemistry is unknown and data for well-characterized defects are scarce and difficult (sometimes impossible) to obtain experimentally. The atomistic processes underlying the evolving defect chemistry and associated quantitative defect properties must be deduced and quantified through numerical simulations.

In the absence of good experimental data that can simultaneously resolve defect structure and electrical behavior—a problem for GaAs—first-principles quantum mechanical methods, within the framework of density functional theory (DFT) [2,3], are needed to predict the structural and electronic properties of defects. Historically, DFT calculations have lacked the necessary accuracy to fill the gaps in defect physics models, both because the physical approximations lacked sufficient fidelity and because of prohibitive computational cost. Theory was fundamentally limited by the accuracy of the functionals, *i.e.*, the effective many-body

interactions between electrons. Conventional DFT, afflicted by a famous “band gap problem”, is seen to severely underestimate band gaps [4]. Conventional computational models within a supercell approximation lacked the rigorous boundary conditions for charged defect simulations, needed to evaluate accurate electron/hole capture energies. Simulations required large computational models, several hundreds of atoms, entailing exceedingly expensive, often prohibitive calculations, and potentially hundreds of these massive calculations are needed. Together, these various shortcomings limited the utility (and reliability) of atomistic DFT simulations as a basis for enabling quantitative assessments of device radiation response.

In this paper, I use first-principles atomistic simulations to elucidate the likely defect evolution after irradiation: identify the initial mobile species in irradiated Si-doped (*n*-type) and C-doped (*p*-type) GaAs, deduce the resulting defect chemistry reaction networks, and predict the associated quantities that characterize the radiation-induced defect chemistry responsible for short-term transient radiation damage. I describe how the simulations results are verified and validated, in an incremental process that provides quantitative confidence of the predictions of defect properties in progressively less-well characterized systems. Atomistic simulations thereby provide the foundation for fully mechanistic, atomistically-informed multiscale predictions of radiation effects on HBTs.

## **COMPUTATIONAL DETAILS**

The defect calculations and analysis in this paper use the methods described in previous works [5,6,7]. In particular, the calculations of dopant and defect complexes are done using the identical computational model and procedures used in a comprehensive study of simple intrinsic defects in (undoped) GaAs [7]. The current calculations of defects involving C and Si dopant

atoms correspond to the simulation context identified as “LDA” in that work. Salient details specific to this work are repeated here, additional details can be found in the previous work.

The density functional theory calculations of defects were performed with SEQQUEST [8], a periodic pseudopotential code using a linear combination of atomic orbitals (LCAO) basis set comprised of contracted Gaussian functions. We improved the parallel capabilities in the code SEQQUEST code to tackle large simulations efficiently, enabling routine calculations of hundreds of multi-hundred atom computational models. We developed new methods to incorporate a rigorous treatment of charged boundary conditions [9] and demonstrated (validated) this approach accurately predicts defect energy levels in extensive comparisons with experimental data in a detailed study of silicon defects [5]. These simulations have since been extended to a broad computational survey of simple intrinsic defects in GaAs [7], to characterize all the simple defects comprising the initial damage products from radiation. Computational models were carefully verified with respect to atomic potentials [6], computational model size, and other considerations specific to DFT simulations [10].

The results presented in this paper used the local density approximation (LDA) within the Perdew-Zunger parameterization [11] to represent the many-body (exchange and correlation) interactions amongst the electrons. Pseudopotentials (PP) were used to replace the effect of core electrons. Both Ga and As used Hamann generalized norm-conserving PP [12] in the “semi-local” form, *i.e.*, without transforming into separable potentials. The PP used were the same described and proven successful in previous studies in GaAs [6,7]. The As atom had a  $Z=5$  valence potential:  $s^2p^3$  valence electrons, with partial core correction, and using a hard  $f$ -electron potential as the local potential. Noting the only minor differences between results including the  $3d$  electrons in the core or in the valence [7], I use the less computationally demanding  $3d$ -core

PP for Ga. The PP for carbon and silicon (both  $Z=4$ ,  $s^2 p^2$  valence) are the same as used previously in studies of defects in silicon [5]. Highly optimized valence double-zeta plus polarization basis sets (two radial degrees of freedom for the strongly-occupied  $s$ - and  $p$ -orbitals, one for weakly-occupied  $d$ -orbitals) are used on all atoms. This procedure produced results in good agreement with other comparable (*i.e.*, well-converged) calculations of formation energies for neutral intrinsic defects in GaAs [7], and defects in silicon [5], and should also be satisfactory for the carbon and silicon defects in GaAs of interest in this paper.

As in previous work [7], defect formation energies are quoted in the arsenic-rich limit: the As chemical potential is set to the energy of an As atom in the  $A7$ -structure bulk elemental crystal and Ga chemical potential to an energy that then produces a zero formation energy for the GaAs perfect crystal. Knowing the theoretical heat of formation, 0.74 eV [7], this can straightforwardly be converted to a Ga-rich ( $A11$  structure) limit [13]. The carbon and silicon chemical potentials are set to the computed energy of each atom in their respective elemental bulk diamond structures. These are arbitrary, only the relative energies of different defects are meaningful.

The GaAs defect calculations are done in cubic 216-site supercells, a  $3 \times 3 \times 3$  scaled version of the smallest GaAs cubic (8-atom) cell, and the Brillouin zone was sampled with a  $2^3$   $k$ -point grid. The computational models used the theoretical GaAs lattice parameter, 0.5599 nm, to prevent any artificial strain effects in the defect calculations. This agrees well with the experimental lattice constant, 0.565 nm [14], as does the computed bulk modulus, 0.724 Mbar, with its measured value, 0.79 Mbar [14]. The atomic structure of each defect was energy-minimized to relax the largest force on any atom to less than 0.1 eV/nm, sufficient to ensure defect total energies are converged to much less than 0.01 eV.

The formalism of the finite defect supercell model (FDSM) [5] was used to provide an accurate method for computing total energies in periodic supercells having net charge. Proper boundary conditions for solving the Poisson Equation for the Coulomb potential in supercell calculations with charged defects are imposed using the local moment countercharge {LMCC} method [15,7]. The chemical potential of a net charge is fixed to a common electron reservoir set by a perfect crystal electrostatic potential [9]. Defect state electron occupations consistent with an isolated defect state are obtained using the discrete defect occupation scheme [5]. The long-range bulk dielectric screening response (the supercell only describes screening within its volume) is evaluated using a simple model [16] for long range polarization. This integrated sequence of procedures was shown to be well-converged to the infinitely dilute bulk limit (within  $<0.05$  eV) for a comprehensive set of intrinsic defects in GaAs [7].

## **VERIFICATION AND VALIDATION STRATEGY**

A sequence of challenges must be overcome for first-principle calculations of defects properties to play a meaningful (i.e., quantitative) role in predictive simulations of device response. The approach taken in this paper is to tackle these challenges incrementally, establishing confidence in each step through careful verification and validation, and assessment of the meaningful errors and uncertainties.

The first of these challenges stems from the recognition that conventional methods for DFT calculations of defects in semiconductors (and oxides) have historically failed to yield quantitative accuracy for defects energies and, in particular, for defect energy levels. The capture of carriers, holes and electrons, within the evolving ensemble of defects after a displacement cascade alters the currents—and hence the gain—in devices such as HBTs. The defect level position are incorporated into the formation energies of defects as a function of the

Fermi level in the gap, thereby influencing the chemical evolution of the defect ensemble. One component of this failure is the “band gap problem” of DFT, where the band states eigenvalue spectrum of DFT is seen to be smaller than the experimental band gap, sometimes much smaller [4]. As the band gap defines the relevant energy scale for defect levels, a flawed band gap energy (computed to be 0.5-0.6 eV for Si [5] and 0.1-1.1 eV for GaAs [6], depending on the formulation of the DFT and associated PP, *c.f.* experimental band gaps of 1.2 and 1.52 eV, respectively), seemingly dictates large errors in defect levels. The issue is whether the physical approximations of DFT are accurate enough for semiconductors applications.

A second component of this failure is the use of the supercell approximation, illustrated in Figure 1. Simulations with DFT use a supercell approximation to represent a defect, where a single defect is replicated periodically in three dimensions. In a supercell approach, the periodic array of charges leads to a divergent Coulomb potential. Once you insert an infinity into any computational model, it is theoretically difficult to remove it again and extract reliable quantities. Nieminen discusses these issues in detail and summarizes various approaches to tackle them [17]. Castleton and Mirbt [18] illustrate the challenges of extracting useful quantities from DFT supercell calculations, estimating the (large) uncertainties that arise when one attempts to extrapolate to the infinitely dilute bulk limit using a numerical fit to a sequence of supercells of increasing size. The issue is whether the computational models to express DFT are accurate enough numerically to satisfy requirements.

The first challenge, therefore, is to develop a computational method that can reliably (verifiably) compute defect properties in the infinite bulk limit, that also has the needed physical accuracy, *e.g.*, does not encounter a band gap problem.

The second challenge stems from the need to have a carefully documented trail of verification and validation for any data that enters into a multiscale formal assessment of radiation response. Given the problematic history of DFT for semiconductors, the onus is particularly exacting. Meaningful validation must be demonstrated with the rather limited well-characterized defect data available in GaAs. Other III-V compounds, *e.g.* InP and GaP, have even less data to validate against (and data is almost non-existent for the ternary alloys employed in most HBTs). The second challenge, therefore, is to provide a chain of evidence that verifies the DFT approach, validates it sufficiently against experimental measurements, and provides some defensible estimate of the errors in the predicted values, for uncertainty quantification.

The strategy to overcome these challenges and establish a verified, validated radiation defect chemistry in GaAs with credible uncertainties follows an incremental path, that permits targeted verification and validation for individual components of the computational approach. The first step was to develop a computational model for computing defect properties the infinite bulk limit, establishing verification for each component. The path to establishing validation of the physical approximation for defect results for GaAs began with—was founded upon—simulations of defects in silicon. The data in GaAs is limited, but the data for defects and defect chemistry in silicon is extensive, detailed, and defect-specific, providing an invaluable proving ground for any defect modeling method, a benchmark to assess the errors of the physical approximations and uncertainties of the resulting predictions. The next step is to apply the principles developed for silicon defect for use in simulations of GaAs defects, taking maximum advantage of the limited data in GaAs to demonstrate validation and depending upon the conceptual and numerical foundation established in silicon. Once the approaches are established in GaAs, then we apply the methods to look at the chemical evolution, identify mobile species and defect reaction

networks, the subject of this paper. Once defects simulations GaAs are established, defects in other III-V's (with even less data) need to be tackled, validated and defect chemistry elucidated. With the ultimate goal to describe the defect evolution in ternaries, such as AlGaAs, with a confidence built up upon an established framework that includes GaAs and AlAs.

## ACHIEVING UNCERTAINTY QUANTIFICATION

The first challenge involved overcoming the formal difficulties posed by the use of the supercell approximation to model charged defects. A sequence of physically motivated, carefully verified formalisms, conceptually illustrated in Figure 2, was formulated and implemented in to the SEQQUEST code [8], to build a series of mathematical bridges between the periodic supercell calculation of a charged defect, Fig.2(b), to a rigorous computational model, Fig. 2(e) of an isolated defect with a net charge, Fig. 2(a). The infinity due to a defect interacting with a periodic array of charges is explicitly avoided with a local-moment counter-charge (LMCC) approach to the solution of the Poisson Equation: the charge is solved with a local potential and only a neutral supercell charge remains for the periodic potential [15], as in Fig. 2(c). This hybrid approach for the electrostatic potential was verified, shown to give the exact Coulomb potential for atoms and molecules with net charge [15]. Referencing the electron potential to a perfect crystal potential, Fig. 2(d), was verified through calculations of defects in NaCl crystals in supercells of different sizes, shapes, and dimensionality [9]. A DFT calculation needs to include the bulk polarization effects of the volume outside of the supercell to give full treatment of the electrostatics, and the energy contribution to the defect energy proves to be well-approximated with a simple analytic formula [5] of the bulk dielectric, illustrated in Fig. 2(e). By itself, none of these steps suffices to give an accurate solution. Developed incrementally, each step could be mathematically formulated and rigorously tested and verified, and,

collectively, a Finite Defect Supercell Model (FDSM) provides a rigorous theoretical framework for defect simulations. With enhanced parallel implementation in the SEQQUEST code, and increasingly powerful computers, the multitudes of large-scale supercell models needed to quantitatively demonstrate the convergence of the defect results to the infinitely dilute bulk limit could be demonstrated [5,7]. With the numerical issues controlled, the next issue is to assess the fidelity of the physical approximations.

The FDSM approach was applied in an extensive computational survey of defects in silicon [5]. The self-interstitial and vacancy are of specific interest to fill notable gaps in defects physics models. Calculations extended to the divacancy and a wide range of different impurity defects and complexes for which good data existed—the *A*-center ( $O_{Si}$  substitutional), nitrogen substitutional, carbon and boron interstitials, phosphorus- and boron-vacancy pairs—to establish validation and to obtain estimates of the errors in the DFT predictions. The computed defect levels, using standard DFT functionals with the LDA and GGA, spanned the band gap, showing no sign of a band gap problem. Moreover, the average deviation from available experimental defect levels was  $\sim 0.1$  eV, and the largest deviation from experiment for any defect defect level was 0.20-0.25 eV, over a sampling of more than 20 different defects levels, both validating the approach and providing a credible estimate of the uncertainties in the predictions of defect levels with DFT.

The approach was then applied to simple intrinsic defects in GaAs [7]. Once more, despite a formal DFT band gap of 0.1-1.1 eV, the range of computed defect levels in GaAs spanned a range consistent with the experimental band gap. The calculations reproduced, to within 0.1 eV, the only firmly identified defect in GaAs, the  $As_{Ga}$  antisite with the EL2 [19, 20], with a midgap donor state and second donor state 0.25 eV lower in the gap [21,22]. On the strength of the

quantitative computed defect levels, the defects associated with the E1-E2 and E3 could be reassigned to the divacancy and As vacancy, respectively [7,23]; the predicted levels lie less than 0.1 eV from their experimentally observed positions. The GaAs calculations are validated against all available quantitative data, with agreement on a order of 0.1 eV, exhibiting the same accuracy, and presumably the same uncertainties, as seen for the more extensive validation suite of defects in silicon. With quantitative confidence in the simulation methods now established for defects in GaAs, the foundation is in place to map the radiation-induced transient defect chemistry in GaAs.

## RESULTS

Mapping the chemical networks responsible for the transient effects in radiation damage begins with identifying the species that are mobilized in the displacement damage following a radiation event. Unlike in silicon, with many mobile defects at accessible temperatures (with a consequently complex chemistry), the calculations in GaAs reveal very few candidate defects that will be mobile. The highly ordered binary structure leads to more complicated, high-energy diffusion pathways, both vacancies,  $v_{\text{Ga}}$  and  $v_{\text{As}}$ , for example, involve migration barriers  $>1$  eV [24,25] that are insurmountable in reasonable device operating conditions. The computational survey of intrinsic defects in GaAs [7] indicated that only the interstitials,  $\text{Ga}_i$  and  $\text{As}_i$ , are possible candidates for the mobile species responsible for any transient effects.

The  $\text{Ga}_i$  can only take positive charge states, preferentially sits in tetrahedral interstices in the lattice, and can migrate between neighboring interstices either via (roughly hexagonal) interstitial channels or via a kick-out mechanism where the Ga interstitial pushes a Ga lattice atom (through a 110-split Ga-pair configuration) into a neighboring interstitial site. The barrier energies for these processes are quoted in Table 1.

**Table 1.** Computed LDA migration energy barriers (eV) for  $\text{Ga}_i$  through different pathways

Barrier site	$\text{Ga}_i(1+)$	$\text{Ga}_i(2+)$	$\text{Ga}_i(3+)$
Hexagonal	1.22	0.79	0.63
$110_{\text{Ga}}$ -split	1.12	0.94	1.00

In *n*-type material, with barriers  $\sim 1$  eV,  $\text{Ga}_i(1+)$  is likely to be immobile. In *p*-type GaAs, the  $\text{Ga}_i(3+)$  might be thermally mobile, having a barrier of only 0.6 eV through the non-bonded hexagonal interstitial channels as it hops from tetrahedral interstice to the next interstice.

Any transient behavior in GaAs, however, is likely to be mediated by the arsenic interstitial. Computed migration barriers for thermal diffusion of  $\text{As}_i$  in *p*-type GaAs are 0.4 eV [7], e.g., the  $\text{As}_i(3+)$  ground state, in a tetrahedral interstice (with As near-neighbor lattice sites) travels through a hexagonal interstice into a neighboring tetrahedral interstice (with Ga near-neighbor lattice sites). Likely diffusion paths (and hence migration barriers) have not been identified for all the accessible charge states ranging from  $\text{As}_i(3+)$  to  $\text{As}_i(1-)$ , but the relatively flat energy landscape over different atomic configurations in all of these suggests possible thermal mobility of  $\text{As}_i$  in *n*-type GaAs as well. The computed thermal barrier is in remarkably good agreement with a 0.5 eV migration energy inferred from experimental data [26], representing additional validation of the simulation results. This lends additional credence for the prediction of a thermal barrier for  $\text{Ga}_i$  diffusion, for which there is no confirmed experimental measurement.

The results further indicate that  $\text{As}_i$  will migrate through an athermal process [27,28]. Sequential capture of electrons and holes drives the atom from a ground state configuration for one charge state (e.g., tetrahedral interstice for  $\text{As}_i(3+)$ ) into a different ground state configuration (hexagonal interstice for  $\text{As}_i(2+)$ ) upon capture of a charge carrier, leading to net

current-driven transport. Carriers to drive this diffusion are present in the normal operation of the device, but copious carriers are also generated during radiation damage and; hence, athermal diffusion is likely to be a prominent, perhaps dominant, source of transient effects.

Any transient radiation damage will begin primarily with athermal  $As_i$ , with a secondary contribution from thermal diffusing  $As_i$ , and with possible contribution of a thermally mobile  $Ga_i$ . These species initiate a defect chemical reaction network, the targets of which will be other defects and impurities in the GaAs material. Certainly, these interstitials could react with other radiation damage products, finding vacancies and healing the lattice or creating antisite defects. Otherwise, the most common defects present in GaAs will be dopants, and I explore the defect reaction networks that begin with carbon and silicon substitutional defects.  $C_{As}$  is an acceptor that is used to dope GaAs  $p$ -type and  $Si_{Ga}$  is a shallow donor that is used to dope GaAs  $n$ -type.

Both dopants,  $C_{As}$  and  $Si_{Ga}$ , have only a single stable charge state in the defect calculations, the carbon as an acceptor  $C_{As}$  (1-) and silicon as donor  $Si_{Ga}$ (1+). These dopants adopt fully symmetric,  $T_d$  substitutional, atomic configurations, with the neutral charge involving states that embed in the band edges in these LDA calculations (and hence not true defect states). The silicon compensating substitutional,  $Si_{As}$  also is only stable in its acceptor charge state  $Si_{As}$  (1-) in a  $T_d$  configuration. The carbon compensating substitutional,  $C_{Ga}$ , by contrast, can take multiple charge states ranging from (1+) to (1-). The formation energies of charged defects in bulk material is dependent upon the Fermi level, for convenience assumed to lie at the conduction band edge (CB) for  $n$ -type and the valence band edge (VB) for  $p$ -type. The formation energies of the substitutional dopants, and the compensating dopant substituting on the alternate site are presented in Table 2.

**Table 2.** Computed LDA formation energy of substitutional dopants and compensating defects.

(eV)	C <sub>As</sub> (1-)	C <sub>Ga</sub> (1+)	Si <sub>As</sub> (1-)	Si <sub>Ga</sub> (1+)
E <sub>fermi</sub> at CB	1.42	4.56	0.34	0.95
E <sub>fermi</sub> at VB	2.96	3.02	1.88	-0.59

The computed formation energies in Table 2 indicate that carbon preferentially occupies the arsenic (dopant) site for all Fermi levels,  $E_{\text{fermi}}$ , in the gap. The silicon, on the other hand, switches from a preference for the Ga (dopant) site at a Fermi level low in the gap (low doping levels) to a preference for the As (compensating) site as the Fermi level rises toward the CB (*i.e.*, *n*-type GaAs), suggesting that doping of GaAs by silicon will be limited by a occupation of the compensating site. This effect has been recognized and evaluated earlier [29]. Accurate reproduction of this effect with these calculations serves to validate the current simulations for dopant-interstitial defect chemistry.

The reaction of mobile interstitials with the C<sub>As</sub> and Si<sub>Ga</sub> dopants results in four reaction initiation scenarios:



Capture of an interstitial atom type identical to the site type the dopant occupies results in the dopant atom becoming a “simple” interstitial, as in reaction (1) and (4). Capture of the other interstitial atom type results in a complex interstitial (pair-substitutional), as in Eq. (2) and Eq. (3). The remainder of this paper focuses on these dopant—interstitial complexes. Compensating

substitutionals,  $C_{Ga}$  and  $Si_{As}$ , are present in GaAs in much lower concentration than dopant substitutionals. Their interactions with interstitials are likely to be less important for radiation response and are neglected here, although it would be straightforward to extend this analysis to include these less likely events. An extensive exploration of possible atomic configurations and stable charge states was performed for each new defect in the ensuing reaction networks to find the ground state structures. A comprehensive listing of all these configurations is impractical (for the  $(SiAs)_{Ga}$  complex alone, over 100 different configurations were screened). The results below quote results from the ground state for each defect, along the thermodynamic chemical pathways important for a defect reaction network.

In C-doped *p*-type GaAs, the  $As_i$  will react exothermically with a  $C_{As}$  dopant, creating a carbon interstitial,  $C_i$ , as in Eq. 1. The  $C_i$  is predicted to have stable charge states ranging from (2+) to (2-), with different structures for different charge states, and each of these charge states has multiple low-energy structures competitive with its ground state. This suggests that  $C_i$ , like the  $As_i$  which created it, will be highly mobile, and not the conclusion of this defect reaction network. As for  $As_i$ , the most likely target for a mobile  $C_i$  are common defects and dopants. It will annihilate any vacancy it encounters in the damage cascade. More interestingly, it can find a second  $C_{As}$  dopant and form a carbon dimer substitutional on the arsenic site,  $(C_2)_{As}$ , in a highly exothermic defect reaction. This dimer is electrically active, taking multiple charge states ranging from (1+) to (1-). A search for structural alternatives found no competitive structures other than a bound  $C_2$  dimer. The  $(C_2)_{As}$  is strongly bound and not mobile and this, therefore, concludes the defect reaction network instigated by  $As_i$ -dopant interactions. Table 3 summarizes the reaction energies ensuing from interstitial-dopant reactions in C-doped, *p*-type GaAs. The thermodynamic reaction energies are presented, using the charge state for each defect

appropriate to the doping. For each reaction, electrons are drawn from the Fermi level to balance the charge.

Table 3: Primary and secondary defect reactions and reaction energies in C-doped (*p*-type) GaAs. Thermodynamic reaction energies are quoted assuming exchange of electrons with the Fermi level at the valence band edge. Negative energy denotes an exothermic reaction.

Reaction	Energy (eV)
$\text{As}_i[3+] + \text{C}_{\text{As}}[1-] + 0e \longrightarrow \text{C}_i[2+]$	-1.35
$\text{C}_i[2+] + v_{\text{As}}[3+] + 6e \longrightarrow \text{C}_{\text{As}}[1-]$	-3.76
$\text{C}_i[2+] + v_{\text{Ga}}[3+] + 4e \longrightarrow \text{C}_{\text{Ga}}[1+]$	-3.15
$\text{C}_i[2+] + \text{C}_{\text{As}}[1-] + 0e \longrightarrow (\text{C}_2)_{\text{As}}[1+]$	-3.23
$\text{Ga}_i[3+] + \text{C}_{\text{As}}[1-] + 2e \longrightarrow (\text{CGa})_{\text{As}}[0]$	-0.16
$(\text{CGa})_{\text{As}}[2+] - 2e \longrightarrow \text{Ga}_{\text{As}}[2+] + \text{C}_i[2+]$	+1.65
$\text{Ga}_i[3+] + \text{As}_{\text{Ga}}[2+] + 2e \longrightarrow \text{As}_i[3+]$	-0.28

The Ga interstitial will also react with the carbon dopant, as in Eq. 2, to form a C-Ga pair-substitutional,  $(\text{CGa})_{\text{As}}$ , C and Ga sharing the same site. This complex, however, is only weakly bound. To emit a carbon interstitial, leaving behind a gallium antisite  $\text{Ga}_{\text{As}}$  would require 1.65 eV energy, so this complex will not dissociate to create a mobile  $\text{C}_i$ . The binding energy to re-emit  $\text{Ga}_i$  is small, and potentially thermally accessible, indicating that the defect reaction network should be explored further. Another common defect in typical As-rich GaAs is the arsenic antisite  $\text{As}_{\text{Ga}}$ , offering another possibility for a sink for  $\text{Ga}_i$ . And, indeed, this reaction is exothermic, if only slightly, but creating what has already been identified as a highly mobile  $\text{As}_i$ . This  $\text{Ga}_i$ -instigated chemistry links into the  $\text{As}_i$ -instigated chemistry described above, hence, completing a candidate defect reaction network. Validating this branch of the reaction network

could prove challenging, as it may not be possible to distinguish it from the primary  $\text{As}_i$ -instigated defect chemistry.

The computed defect reaction energies ensuing from interstitial-dopant reactions in the predicted reaction network in Si-doped  $n$ -type GaAs are presented in Table 4.

Table 4: Primary and secondary defect reactions and reaction energies in Si-doped ( $n$ -type) GaAs. Thermodynamic reaction energies are quoted assuming exchange of electrons with the Fermi level at the conduction band edge. Negative energy denotes an exothermic reaction.

Reaction	Energy (eV)
$\text{As}_i[1-] + \text{Si}_{\text{Ga}}[1+] + 0e \longrightarrow (\text{SiAs})_{\text{Ga}}[0]$	-0.70
$(\text{SiAs})_{\text{Ga}}[0] + 2e \longrightarrow \text{As}_{\text{Ga}}[0] + \text{Si}_i[2-]$	+2.20
$\text{Ga}_i[1+] + \text{Si}_{\text{Ga}}[1+] + 4e \longrightarrow \text{Si}_i[2-]$	-0.92
$\text{Si}_i[2-] + \nu_{\text{As}}[3-] - 4e \longrightarrow \text{Si}_{\text{As}}[1-]$	-5.37
$\text{Si}_i[2-] + \nu_{\text{Ga}}[3-] - 6e \longrightarrow \text{Si}_{\text{Ga}}[1+]$	-2.88
$\text{Si}_i[2-] + \text{Si}_{\text{Ga}}[1+] + 0e \longrightarrow (\text{Si}_2)_{\text{Ga}}[1-]$	-1.79
$(\text{Si}_2)_{\text{Ga}}[1-] + 0e \longrightarrow (\text{SiSi})_{\text{GaAs}}[0] + \text{As}_i[1-]$	+0.60

The arsenic interstitial reacts with a  $\text{Si}_{\text{Ga}}$  dopant to form a stable  $(\text{SiAs})_{\text{Ga}}$  complex, bound by 0.70 eV. A plausible continuation would be to emit silicon interstitial,  $\text{Si}_i$ , to leave behind an  $\text{As}_{\text{Ga}}$  antisite, a particularly stable defect in GaAs. The calculations indicate this would require more than 2 eV, making this dissociation reaction impossible at typical device temperatures. The Si-As substitutional complex terminates the  $\text{As}_i$ -instigated chemistry.

The  $\text{Ga}_i$ - $\text{Si}_{\text{Ga}}$  reaction network in  $n$ -type GaAs mirrors the  $\text{As}_i$ - $\text{C}_{\text{As}}$  reaction network in  $p$ -type GaAs. The Ga interstitial displaces a  $\text{Si}_{\text{Ga}}$  dopant, creating a Si interstitial, downhill by 0.9 eV. The  $\text{Si}_i$  is itself likely to be highly mobile. It has a flat energy landscape, with prospects for

thermal diffusion, and multiple structural bistabilities with changing charge state, suggesting a susceptibility to athermal diffusion. It will annihilate any vacancy it finds, of course. Like the  $\text{Ga}_i$  which created it, the  $\text{Si}_i$  will react with a(nother)  $\text{Si}_{\text{Ga}}$  dopant. This reaction is also significantly exothermic, creating a strongly bound defect complex, one that cannot diffuse. The second Si could conceivably push out a second lattice atom, a nearby As site, emitting an arsenic interstitial and leaving behind a pair of Si atoms on neighboring sites. While not predicted to be favorable, this could perhaps be thermally accessible (especially accounting for the 0.1-0.2 eV uncertainties in DFT-based defect energies asserted above). This terminates the  $\text{Ga}_i$ -initiated defect reaction network in Si-doped GaAs.

## SUMMARY AND CONCLUSIONS

The defect reaction networks required to describe the short-time transient response of irradiated GaAs have been developed using atomistic simulation methods. The results of first-principles atomistic simulations based on density functional theory identified the mobile species generated by the initial displacement damage, guided the search for the ensuing defect reaction pathways, and quantified the associated defect formation and reaction energies for defect chemistries likely to be responsible for transient behavior. Mobile self-interstitials, and particularly the cation (arsenic) interstitial, are likely responsible for short-time transient behavior. For both *p*-type (C-doped) and *n*-type (Si-doped) GaAs, the defect chemistry instigated by these radiation-mobilized interstitials was elucidated, following each candidate reaction network to each likely terminus, computing the defect reaction energies for each reaction in the network. The chemical networks constructed here are crucial to define the reaction networks that enable device simulations to simulate electrical response of entire irradiated devices, and would be difficult (perhaps impossible) and time-consuming (expensive)

to elicit from purely experimental studies. Following a deliberate strategy to verify and validate the results of the simulations, these simulations are now able to define the form of the chemistry needed for device simulations and populate those defect physics models with physically reliable parameters with the necessary quantitative confidence. The current results focused on formation and reaction energies of defects, further simulations would be needed to predict the migration barrier energies and reaction barriers for the mobile species, values needed by device codes to simulate the influence of evolving the defect chemistry on device response. While simulations do provide a wealth of information, targeted experiments are crucial to validate the predicted chemistries. The simulations provide a guide for where experiments can be focused most effectively.

Extending these calculations of defects in GaAs to AlAs [30], and also to InP and GaP [23], the path to developing the radiation defect physics in the ternary alloys (e.g., AlGaAs or InGaP) is open, offering the possibility that future quantitative assessments of radiation sensitivities in HBT devices can be informed by predictive mechanistic, quantitative descriptions of radiation response, reducing the dependence on phenomenological models and testing. With effective first-principles simulations, careful experiments, and well-motivated device models that incorporate atomistic-aware defect physics, the prospect is bright that radiation effects in HBT (and other) devices can be systematically and quantitatively assessed, using numerical simulations of fundamental physical processes as an essential component.

## **ACKNOWLEDGMENTS**

Sandia National Laboratories is a multi-program laboratory managed and operated by Sandia Corporation, a wholly owned subsidiary of Lockheed Martin Company, for the United States

Department of Energy's National Nuclear Security Administration under contract DE-AC04-94AL85000.

## REFERENCES

1. P. Pilcher, *Intrinsic Point Defects, Impurities, and Their Diffusion in Silicon* (Springer-Verlag, Wien 2004).
2. P. Hohenberg and W. Kohn, Phys. Rev. **136**, B864 (1964).
3. W. Kohn and L.J. Sham, Phys. Rev. **140**, A1133 (1965).
4. L.J. Sham and M. Schlüter, Phys. Rev. Lett. **51**, 1888 (1983); Phys. Rev. B **32**, 3883 (1985).
5. P.A. Schultz, Phys. Rev. Lett. **96**, 246401 (2006).
6. O.A. von Lilienfeld and P.A. Schultz, Phys. Rev. B **77**, 115202 (2008).
7. P.A. Schultz and O.A. von Lilienfeld, Modelling Simul. Mater. Sci. Eng. **17**, 084007 (2009).
8. P.A. Schultz, SEQQUEST code (unpublished). See <http://dft.sandia.gov/Quest/>.
9. P.A. Schultz, Phys. Rev. Lett. **84**, 1942 (2000).
10. A.E. Mattsson, P.A. Schultz, T.R. Mattsson, K. Leung, and M.P. Desjarlais, Modelling Simul. Mater. Sci. Eng. **13**, R1 (2005).
11. J.P. Perdew and A. Zunger, Phys. Rev. B **23**, 5048 (1981).
12. D.R. Hamann, Phys. Rev. B **40**, 2980 (1989).
13. S.B. Zhang and J.E. Northrup, Phys. Rev. Lett. **67**, 2339 (1991).
14. J.S. Blakemore, J. Appl. Phys. **53**, R123 (1982).
15. P.A. Schultz, Phys. Rev. B **60**, 1551 (1999).
16. W. Jost, J. Chem. Phys. **1**, 466 (1933).

17. R.M. Nieminen, *Modelling Simul. Mater. Sci. Eng.* **17**, 084001 (2009).
18. C.W.M. Castleton, A. Höglund, and S. Mirbt, *Modelling Simul. Mater. Sci. Eng.* **17**, 084003 (2009).
19. J. Dambrowski and M. Scheffler, *Phys. Rev. Lett.* **60**, 2183 (1988).
20. D.J. Chadi and K.J. Chang, *Phys. Rev. Lett.* **60**, 2187 (1988).
21. J. Lagowski, D.G. Lin, T.-P. Chen, M. Skowronski, and H.C. Gates, *Appl. Phys. Lett.* **47**, 929 (1985).
22. P. Omling, P. Silverbeg, and I. Samuelson, *Phys. Rev. B* **38**, 3606 (1988).
23. P.A. Schultz, unpublished.
24. F. El-Mallouhi and N. Mousseau, *Phys. Rev. B* **74**, 205207 (2006).
25. F. El-Mallouhi and N. Mousseau, *Appl. Phys. A* **86**, 309 (2007).
26. J.C. Bourgoin, H.J. Bardeleben, and D. Stiévenard, *J Appl. Phys.* **64**, R65 (1988).
27. G.D. Watkins, *Radiation Damage in Semiconductors*, ed. P. Baruch, p97 (Dunod, Paris, 1965).
28. J.C. Bourgoin and J. Corbett, *Phys. Lett. A* **38**, 135 (1972).
29. J.E. Northrup and S.B. Zhang, *Phys. Rev. B* **47**, 6791 (1993).
30. P.A. Schultz, *MRS Symposia Proc.* **1370**, [accepted] (2011).

## FIGURE CAPTIONS

**Figure 1.** Illustration of the supercell approximation used to construct a computational model of defect using periodic bulk density functional theory codes. A physical system with defect bearing a net charge in an infinite bulk medium is mapped onto a computational model where the defect and a finite number of atoms surrounding it are periodically replicated in three dimensions. For a neutral defect, this approaches the bulk limit once the perturbation created by the defect is isolated from its periodic replicas by the inclusion of sufficient buffer atoms. For a charged defect, the periodically replicated charge introduces a mathematical divergence, which makes evaluation of quantitatively meaningful energies difficult.

**Figure 2.** Conceptual illustration of the sequence of formalisms that converts a conventional supercell model (b) into a model representative of the target physical system: an isolated defect. The periodic array of charges (b), and the associated divergence in Coulomb potential are avoided via solving the Poisson Equation for the electrostatic potential treating the net charge as a local potential within the cell (cutting off the potential at the boundary of the cell), treating the remainder of the charge periodically (c). A common energy reference for electron removal, needed to compute reliable defect energy levels, is found by connecting the density and potential to the perfect crystal density and potential (d). Finally, the dielectric screening of the bulk medium outside of the volume of the supercell simulation volume is computed with a simple model, reconstructing a model (e) now representative of a single isolated charge defect (a).

**FIGURE 1**

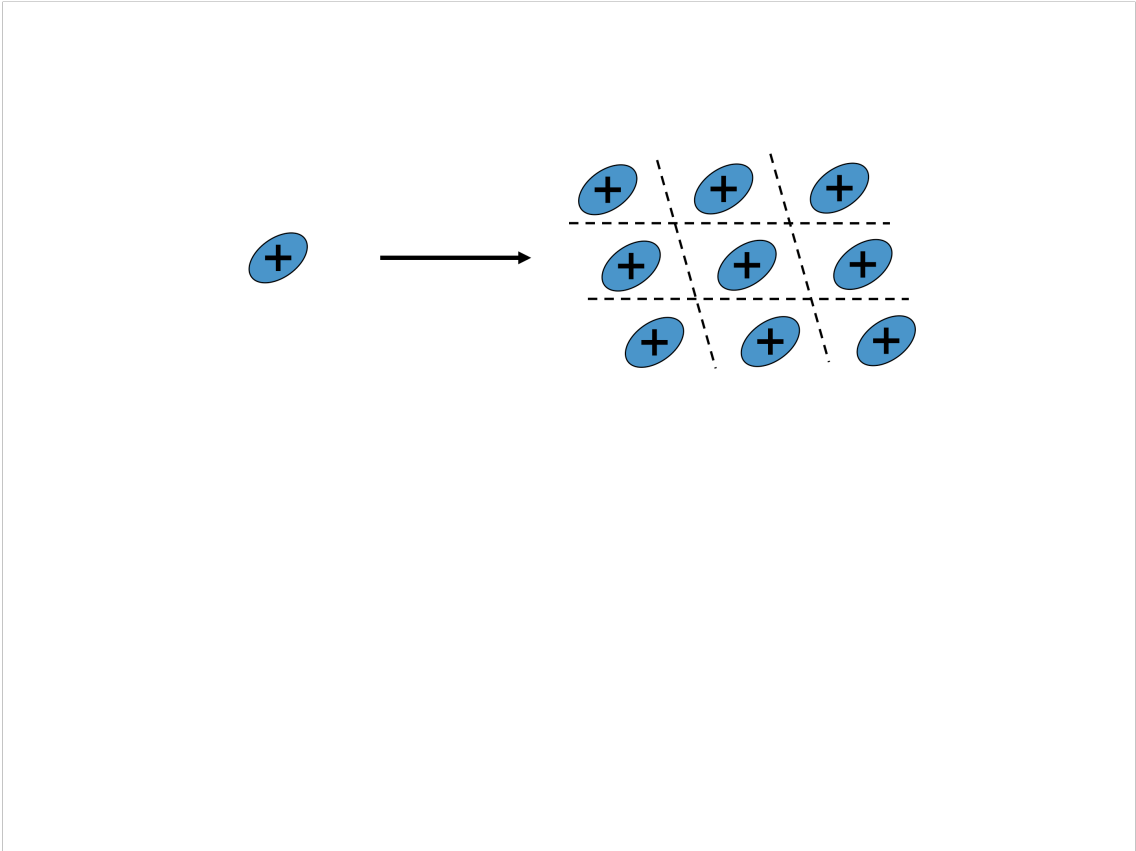


FIGURE 2

